RSC Advances

PAPER

View Article Online
View Journal | View Issue

Cite this: *RSC Adv.*, 2019, **9**, 15124

Role of confining liquids on the properties of Cu@Cu_2O nanoparticles synthesized by pulsed laser ablation and a correlative ablation study of the target surface

Prahlad K. Baruah, Ashwini K. Sharma and Alika Khare *

The effect of confining liquid on the properties of copper nanoparticles synthesized by pulsed laser ablation in two organic solvents, methanol and 2-propanol is investigated along with the effect of the laser irradiation time on the synthesized nanoparticles. To understand the role of confining liquids on the formation mechanism of the nanoparticles in different environments, the results obtained in the organic solvents are compared to those obtained in distilled water. The increase in the average size of the nanoparticles from 7–19 nm with the laser irradiation time from 15–60 minutes is accompanied by a shift in the plasmonic peak towards longer wavelength from 606–621 nm, respectively in methanol. In the case of nanoparticles synthesized in 2-propanol, the average size of the nanoparticles increases from 9–17 nm and there is a corresponding shift in the SPR peak from 581–601 nm, respectively. The increase in the size of the nanoparticles with the increase in irradiation time in the organic solvents is the reverse trend of that obtained for nanoparticles synthesized in distilled water. The range of the plasmonic peak positions is blue shifted for the nanoparticles synthesized in methanol and 2-propanol as compared to that of 626–641 nm for the nanoparticles synthesized in distilled water indicating the formation of insufficiently oxidized nanoparticles in organic solvents. Formation of core–shell spherical copper nanoparticles with carbon encapsulation in methanol and 2-propanol is another interesting observation. The origin of the dependence of properties of the synthesized nanoparticles on the ambient liquid lies in the way the laser beam interacts with the target surface in the ambient. A detailed ablation study on the laser produced crater in all the three liquids is carried out to understand the factors that affect the properties of the nanoparticles.

Received 9th January 2019
Accepted 8th May 2019

DOI: 10.1039/c9ra00197b

rsc.li/rsc-advances

1. Introduction

Noble metals have attracted much attention in recent years due to their remarkable optical, electronic and catalytic properties.[1–4] The surface plasmon resonance (SPR) associated with noble metal nanoparticles (NPs) has facilitated their use in various plasmonic applications.[2,5] The metal oxide NPs, especially those of copper (Cu) are also attracting attention due to some of their fascinating properties.[6–8] Cu oxide semiconductors, possessing narrow bandgaps, are being extensively used in renewable energy production.[9] For instance, Cu_2O thin films are used as hole-transport layers in perovskite solar cells and CuO nanostructures are being used as electrode materials in supercapacitors.[10,11] Both Cu_2O and CuO have potential applications as gas sensors and their photocatalytic activities are found to be excellent.[12,13] However, these properties are dependent on the composition and structure and therefore, it is important to optimize them for various applications.[9] The choice of Cu_2O or CuO depends on the particular application and hence it is essential to control the oxidation of Cu NPs. Controlled oxidation of NPs has been achieved mostly by chemical techniques like chemical vapour synthesis, and also by adjusting the molecular weight of capping molecules.[14,15] As most of these chemical techniques require the use of strong chemical reagents which may prove to be harmful to the environment, therefore, alternate environment friendly techniques are consistently being looked for.

Pulsed laser ablation in liquid (PLAL) is a very efficient technique, normally devoid of any harmful chemicals, for the synthesis of NPs.[16,17] The properties of the NPs formed by this technique can be tuned by varying the laser parameters, target material and also the surrounding liquid medium. Laser ablation in liquid results in high pressure and high temperature regime which induces various chemical reactions between the laser induced target plasma and that of the surrounding liquid. As a result, the structure and composition of the NPs can be controlled easily. There have been reports of synthesis of NPs

Department of Physics, Indian Institute of Technology Guwahati, Guwahati, 781039, India. E-mail: alika@iitg.ac.in; Tel: +91 361 2582705

and controlling its properties in different liquids like ethanol, glycol, acetone, aqueous solution of sodium dodecyl sulfate surfactants, *etc.*[18–21] However, the synthesis of Cu NPs *via* PLAL results in NPs which are prone to oxidation, especially when the synthesis of the NPs is carried out in water.[22] Liu *et al.* reported the reduction in the oxidation of Cu NPs synthesized in oxygen-deficient organic solvents.[18] The formation of an encapsulated carbon layer from the organic liquid over the surface of Cu NPs is believed to be the reason behind the reduced oxidation. The degree of oxidation taking place in the NPs affects its plasmonic response.[23] Although there is a report on blueshift in the SPR peak in the case of ablation in organic solvents as compared to that in pure water, a better and comprehensive study in this area is further required which may be useful in the understanding of the oxidation in the NPs better.[18] It may also be interesting to study the effect of the ambient on the surface of the target itself as the interaction of the laser beam with the target surface is the heart of the entire process. Although there have been numerous correlative studies on the formation mechanism of NPs and the synthesis conditions *via* plasma spectroscopic technique, no attempt has been made to unveil the mechanism of NP synthesis through a proper ablation study of the target surface.[24,25]

In the present work, synthesis of Cu NPs has been carried out in two organic liquids *viz.*, methanol and 2-propanol. The properties of the NPs synthesized in these liquids are also compared to that of NPs synthesized in distilled water (DW), reported earlier.[26] The change in the size and structure of the NPs as a function of laser irradiation time in the liquids is also investigated. In addition, the effect of various ambient on the target surface due to laser irradiation is studied and the material ablation rate is compared. An attempt is made to correlate the observed changes in the target surface due to laser ablation in different ambients and the properties of the NPs.

2. Experimental details

2.1 Synthesis and characterization of NPs

The Cu NPs were synthesized by the ablation of pure Cu target (Cu foil of thickness 0.5 mm, purity 99.98%; Sigma-Aldrich, USA) in methanol and 2-propanol. The Cu target was placed at the bottom of a glass beaker filled with 8 mL of the liquid in each case. The second harmonic of a Q-switched Nd:YAG laser (Model: Litron LPY7864-10G) having a pulse duration of 7 ns was used for ablating the target. The laser was operated at a repetition rate of 10 Hz. The laser beam was suitably steered using a set of optical components and then focused by a 25 cm focal length lens onto the target immersed in the liquid. In order to facilitate the availability of fresh area of ablation for each laser shot, the target was continuously translated with the help of a motorized programmable translational stage. The colloidal solution, containing the ablated NPs and the solvent, was also manually stirred at definite intervals during the ablation process to disperse the NPs formed and hence to enable the laser beam to reach the target unobstructed. The NPs were synthesized for laser ablation duration of 15, 30 and 60 minutes at a fixed laser energy of 30 mJ as reported earlier for synthesis of NPs in DW.[26] The spot size of the laser beam at a laser energy of 30 mJ per pulse is shown in Fig. 1. The corresponding laser ablation fluence is estimated to be $\sim$10 J cm^{-2}. The Cu NPs were characterized by the transmission electron microscope (TEM; JEOL JEM 2100, JEOL JEM 2100F) to ascertain its size, shape and identification of the phase of the NPs. For this, the colloidal solution of the NPs were drop casted onto carbon coated copper grids and were taken for TEM analysis. The SPR of the NPs was studied by recording the absorption spectra of the colloidal solutions using a UV-visible spectrophotometer (Shimadzu UV-3101 PC). The samples were also investigated by the X-ray diffractometer (Rigaku, TTRAX III) operated at a wavelength of 1.5407 Å of Cu-Kα. For this, the NP solutions were drop casted onto silicon wafers and dried and then exposed to the X-rays.

2.2 Laser produced crater and its characterization

In order to investigate the structural and morphological changes of the laser irradiated target surface in various ambients, laser ablation of the Cu surface was performed in air, DW, methanol and 2-propanol. For this, the ablation is carried out under similar conditions as was employed for the synthesis of NPs, with the only difference being that the target is not translated during ablation and repeated shots of laser were fired at the same spot for 5 minutes to produce a prominent crater. The craters produced, as a result of ablation carried out in the different ambients, are characterized by optical microscope (OLYMPUS BX51M), Raman spectrophotometer (Horiba Lab-Ram HR800), Energy Dispersive X-ray (EDX) spectrometer (Oxford Instruments), surface profilometer (Taylor Hobson; Talysurf CCI lite) and Field emission scanning electron microscope (FESEM; Zeiss, Sigma).

3. Results and discussion

The synthesis of Cu NPs in DW as a function of laser irradiation time was reported earlier.[26] The SPR peak of Cu NPs was red-shifted to 626–641 nm range from its usual reported range of 570–580 nm. This red-shift was attributed mainly to the formation of oxidized NPs due to the release of oxygen during

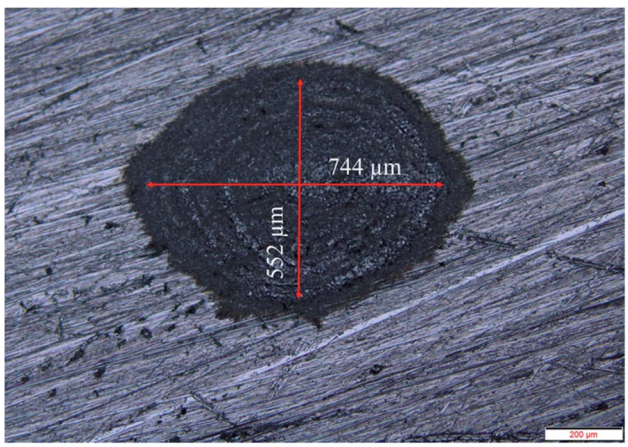

Fig. 1 Laser focal spot size using a 25 cm focal length lens at 30 mJ laser energy per pulse.

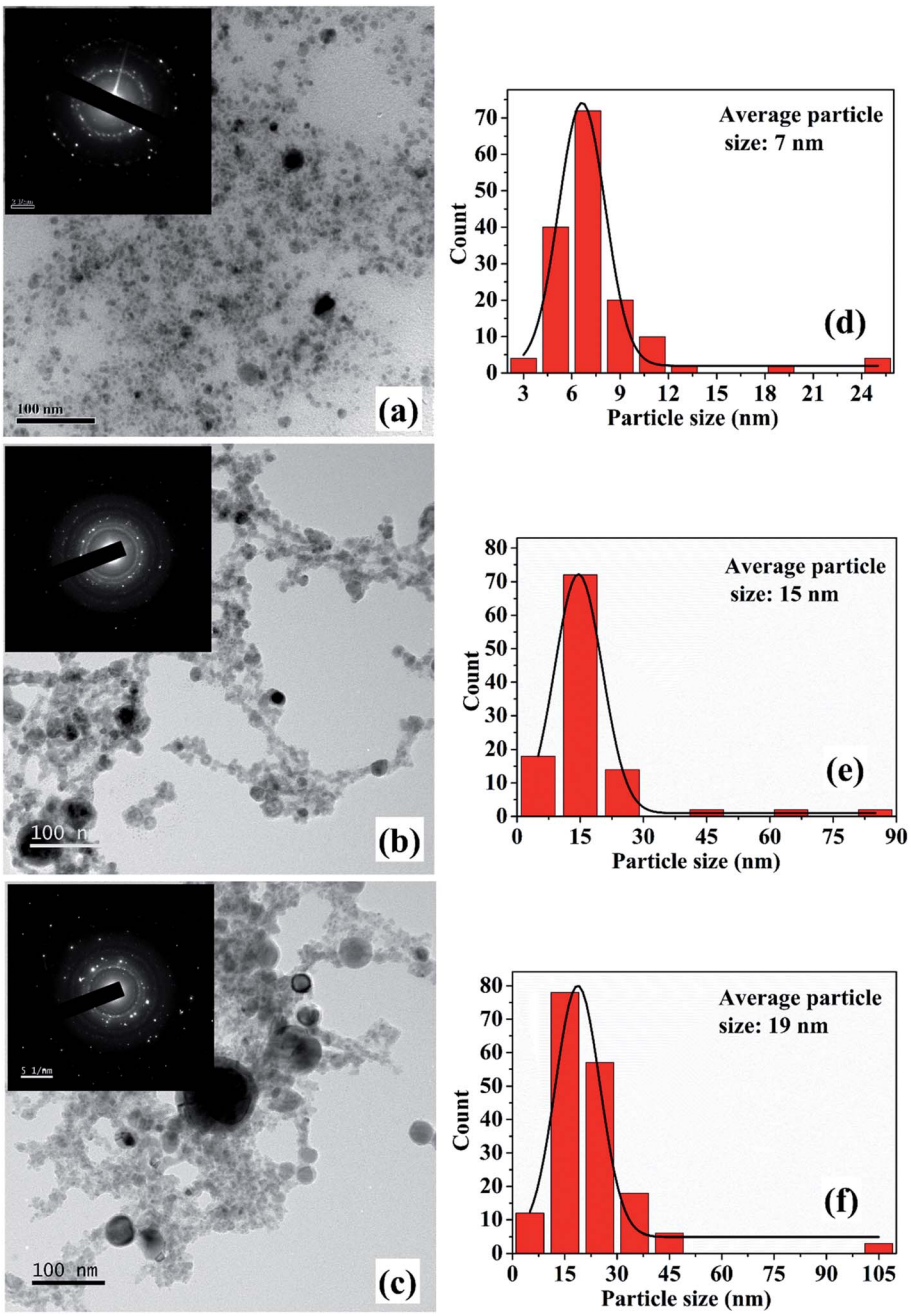

Fig. 2 (a), (b) and (c) TEM images along with the SAED pattern (inset) for Cu NPs synthesized in methanol at incident laser energy of 30 mJ for an irradiation time of 15, 30 and 60 minutes, respectively; (d)–(f) corresponding particle size distribution.

ablation in DW. It was also observed that an increase in laser irradiation time resulted in the formation of smaller and finer NPs. This reduction in the size of NPs was accompanied by a blue-shift in the SPR peak of the samples. The formation of oxidized NPs was also confirmed by Raman studies and the selected area electron diffraction (SAED) patterns which showed definite formation of Cu@Cu_xO ($x = 1, 2$) NPs. It was also observed that for lesser duration of laser irradiation, Cu_2O is the main oxide phase while for longer laser irradiation time of 60 minutes there is an additional CuO phase. The characterization of the NPs synthesized in methanol and 2-propanol is discussed in the following sections.

3.1 Characterization of NPs

3.1.1 Size and structure of Cu NPs. The TEM images along with the SAED patterns (insets) of the samples synthesized in

Table 1 Properties of the chosen liquid in the present study

Ambient	Density (g mL^{-1})	Thermal conductivity (W mK^{-1})	Acoustic impedance (g cm^{-2} s^{-1})
Air	0.001	0.025	42.8
DW	0.998	0.591	1.48×10^5
Methanol	0.791	0.200	0.89×10^5
2-Propanol	0.785	0.135	0.92×10^5

methanol for laser irradiation time of 15, 30 and 60 minutes are shown in Fig. 2(a)–(c), and the corresponding particle size distribution are depicted in Fig. 2(d)–(f), respectively. The particles formed are of nearly spherical shape and the average size of the NPs are found to be ~7, 15 and 19 nm for the irradiation time of 15, 30 and 60 minutes, respectively.

The increase in the size of the NPs with irradiation time is an interesting observation and this variation in size is in contrast to that observed in the case of ablation in DW.[26] For the NPs synthesized in DW, the decrease in its average size with the increase in the laser irradiation time is due to the fragmentation of the initially formed larger particles but the same fragmentation mechanism is not found to be dominant for the NPs synthesized in methanol.[26] The growth of the NPs with the laser irradiation time may be explained on the basis of the mechanism proposed by Zeng *et al.*[27] In their work, the variation in the size of the NPs in terms of the laser irradiation time is explained by considering three stages. In the initial stage, fragmentation of the NPs take place and in the second stage a growth in the size of the NPs is observed. The final stage is characterized by only a slight increase in the size of the NPs. In the case of the NPs synthesized in methanol, with the increase in laser

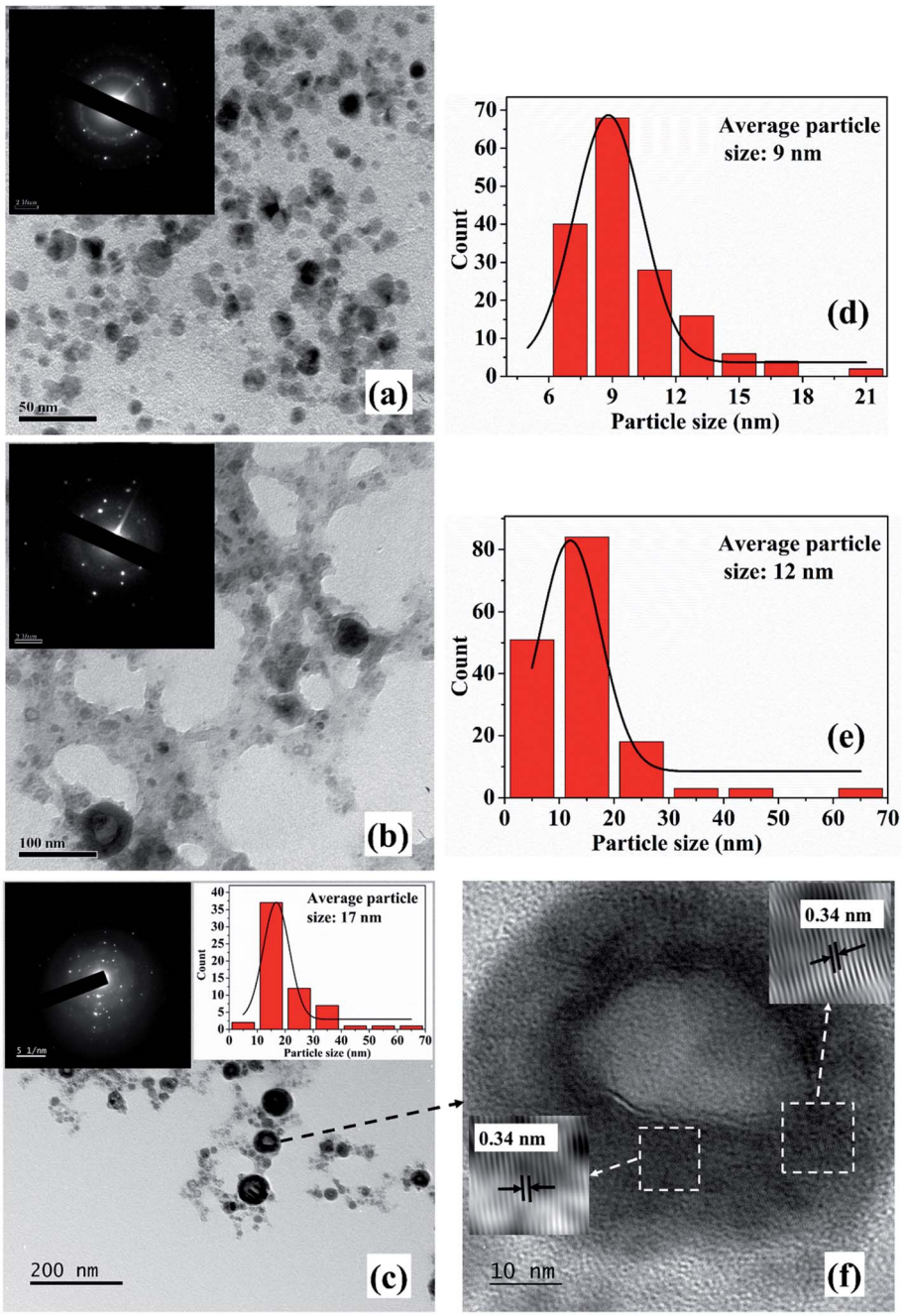

Fig. 3 (a), (b), (c) TEM images along with the SAED pattern (inset) of Cu NPs synthesized in 2-propanol at incident laser energy of 30 mJ for an irradiation time of 15, 30 and 60 minutes, respectively; (d), (e), inset of (c) corresponding particle size distributions; (f) HRTEM image of the sample synthesized with irradiation time of 60 minutes, showing the core–shell structure.

Table 2 *d*-values calculated from the SAED patterns along with corresponding planes for the NPs synthesized in methanol and 2-propanol

		Cu in methanol			Cu in 2-propanol		
hkl planes	*d*-value	15 minutes	30 minutes	60 minutes	15 minutes	30 minutes	60 minutes
Cu (111)	0.20	—	✓	✓	✓	✓	✓
Cu_2O (110)	0.29	✓	—	—	✓	—	—
Cu_2O (111)	0.24	—	—	✓	—	✓	✓
Cu_2O (211)	0.17	✓	—	—	✓	—	—
Cu_2O (220)	0.16	—	—	✓	—	✓	—
Cu_2O (310)	0.13	✓	✓	✓	✓	—	—
Cu_2O (321)	0.11	✓	✓	✓	—	—	—
Cu_2O ($12\bar{4}$)	0.08	—	✓	✓	—	—	—

irradiation time, growth of the NPs is characterized by an increase in the average size of the NPs. At the growth stage, the initially formed particles are transformed into hot plasma. When the plasma cools down, nucleation and growth of these species take place. Coalescence of the ablated species may result in bigger sized particles. This results in an increase in the particle size with longer irradiation time. Thus, the 2nd stage as reported by Zeng *et al.* is found to be the effective stage for the NPs in the present case. The difference in the formation mechanism in methanol and DW lies in the fact that the density of methanol is less than that of DW as listed in Table 1. The higher density of DW provides a more confined atmosphere during laser ablation and as a result fragmentation among the ablated species is dominant in DW. Hence, although there is fragmentation taking place in methanol, the growth of the NPs as mentioned earlier dominates over the fragmentation.

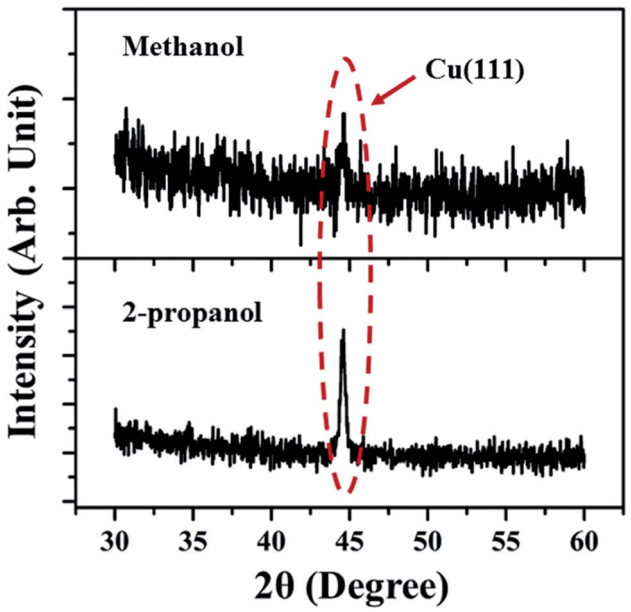

Fig. 4 XRD spectra of Cu NP samples synthesized in methanol and 2-propanol for an irradiation time of 60 minutes.

The TEM images and SAED patterns (insets) of NPs synthesized in 2-propanol for an irradiation time of 15, 30 and 60 minutes are demonstrated in Fig. 3(a)–(c), respectively. The corresponding particle size distribution of the samples are shown in Fig. 3(d), (e) and inset of 3(c), respectively. The average particle size of these samples are found to be 9, 12 and 17 nm, respectively. Similar to the NPs synthesized in methanol, an increase in the average size of the NPs is observed with the increase in the laser irradiation time from 15 to 60 minutes which is again attributed to the lower density of 2-propanol as compared to that of DW. This growth of the NPs in the organic liquids with the increase in laser irradiation time in the present set of conditions is indeed intriguing and is taken up for further studies.

The SAED patterns of the NPs in both the liquids reveal that the synthesized NPs are polycrystalline in nature. The *d*-values

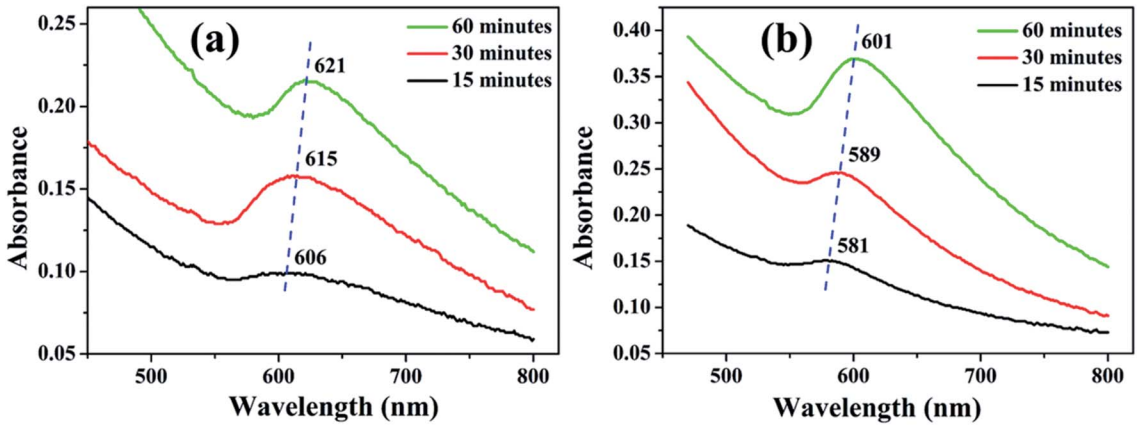

Fig. 5 UV-visible absorption spectra of NPs synthesized in (a) methanol and (b) 2-propanol for irradiation time of 15, 30 and 60 minutes.

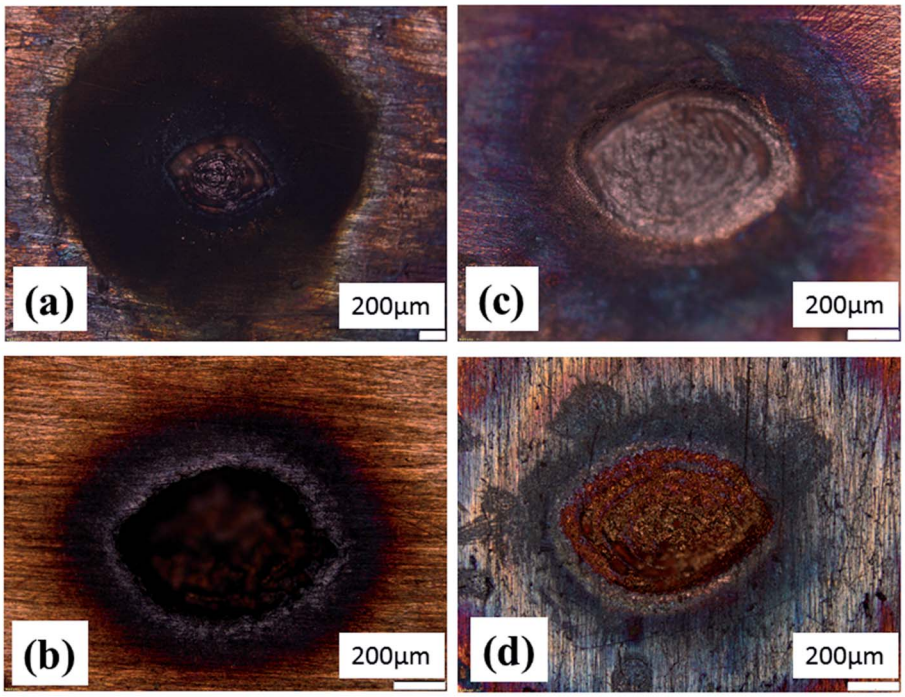

Fig. 6 Optical micrographs of laser ablated crater produced in (a) air, (b) DW, (c) methanol and (d) 2-propanol.

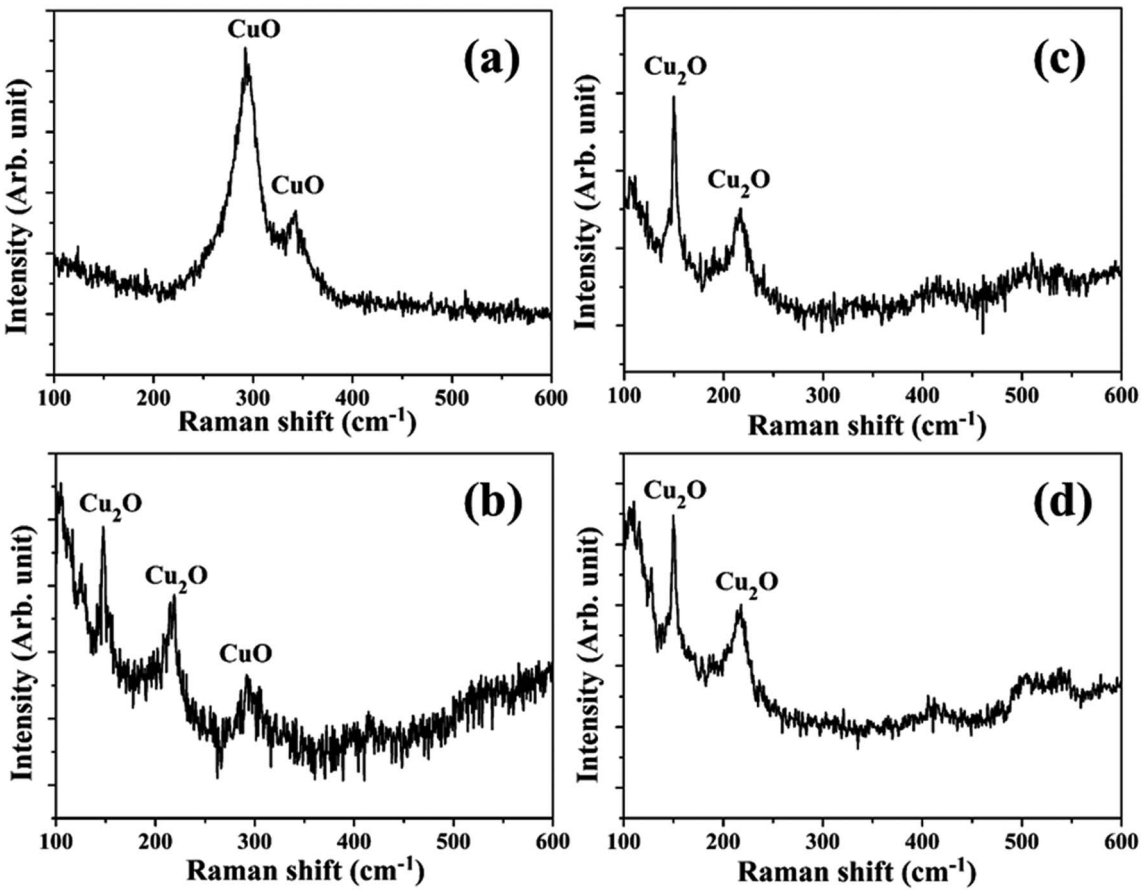

Fig. 7 Raman spectrum in the peripheral region of the laser ablated crater produced in (a) air, (b) DW, (c) methanol and (d) 2-propanol.

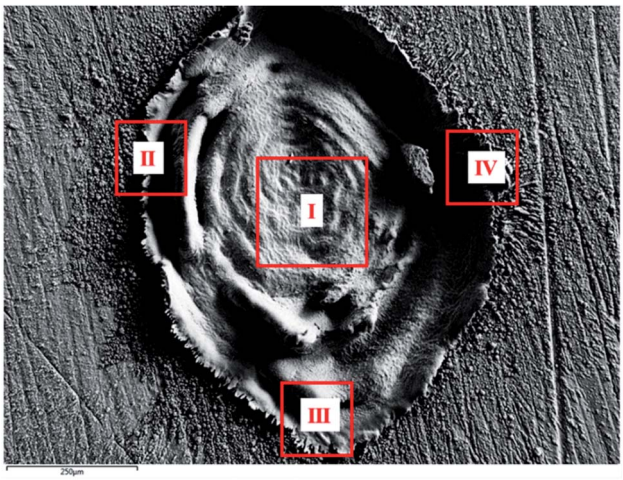

Fig. 8 FESEM image of laser produced crater in air exhibiting the different regions chosen for EDX analysis.

calculated from the diffraction patterns indicate the presence of planes corresponding to Cu_2O phase of the NPs in all the samples in addition to the Cu (111) plane. The details of the crystalline planes observed in the SAED patterns are listed in Table 2. For the NPs synthesized in DW, there was formation of Cu_2O as well as CuO phases of NPs.[26] However, in the case of ablation in methanol and 2-propanol, although there is aerobic transformation of Cu to Cu_2O, no further oxidation to CuO was observed. This confirms that the ablation carried out in oxygen-deficient solvents is useful in reducing the degree of oxidation of the NPs synthesized *via* PLAL.

From the TEM images, it is also observed that there is a formation of core–shell kind of NPs for the samples synthesized for higher irradiation time of 30 and 60 minutes. The formation of core–shell NPs is believed to be due to the encapsulation of the NPs formed initially by the carbon from the surrounding liquid.[18] When laser ablation is carried out in the organic solvents, the number of hydrogen and carbon species generated is more than that of oxygen species due to the lower bond energies of C–C (347 kJ mol^{-1}) and C–H (413 kJ mol^{-1}) as compared to O–H (467 kJ mol^{-1}). The carbon from the solvent encapsulates the Cu NPs formed by the ablation of the Cu target thus favouring the formation of insufficiently oxidized NPs in organic solvents. The carbon encapsulation of the NPs in the synthesis of NPs *via* pulsed laser ablation in organic solvents has been widely reported.[18,20,21]

In order to confirm the carbon encapsulation, the HRTEM image of one of the core–shell NPs synthesized in 2-propanol for 60 minutes of irradiation time is depicted in Fig. 3(f). The HRTEM image clearly shows the lattice fringes corresponding to graphitic carbon ($d \sim 0.34$ nm) surrounding the NPs confirming the carbon encapsulation of the Cu@Cu_2O NPs.

The XRD spectra (Fig. 4) shows the peak corresponding to Cu (111) plane only, which was also detected in the SAED patterns. The absence of oxide phase of the synthesized NPs indicates comparatively small amount of oxidation. However, the SAED patterns due to the electrons is more sensitive as compared to

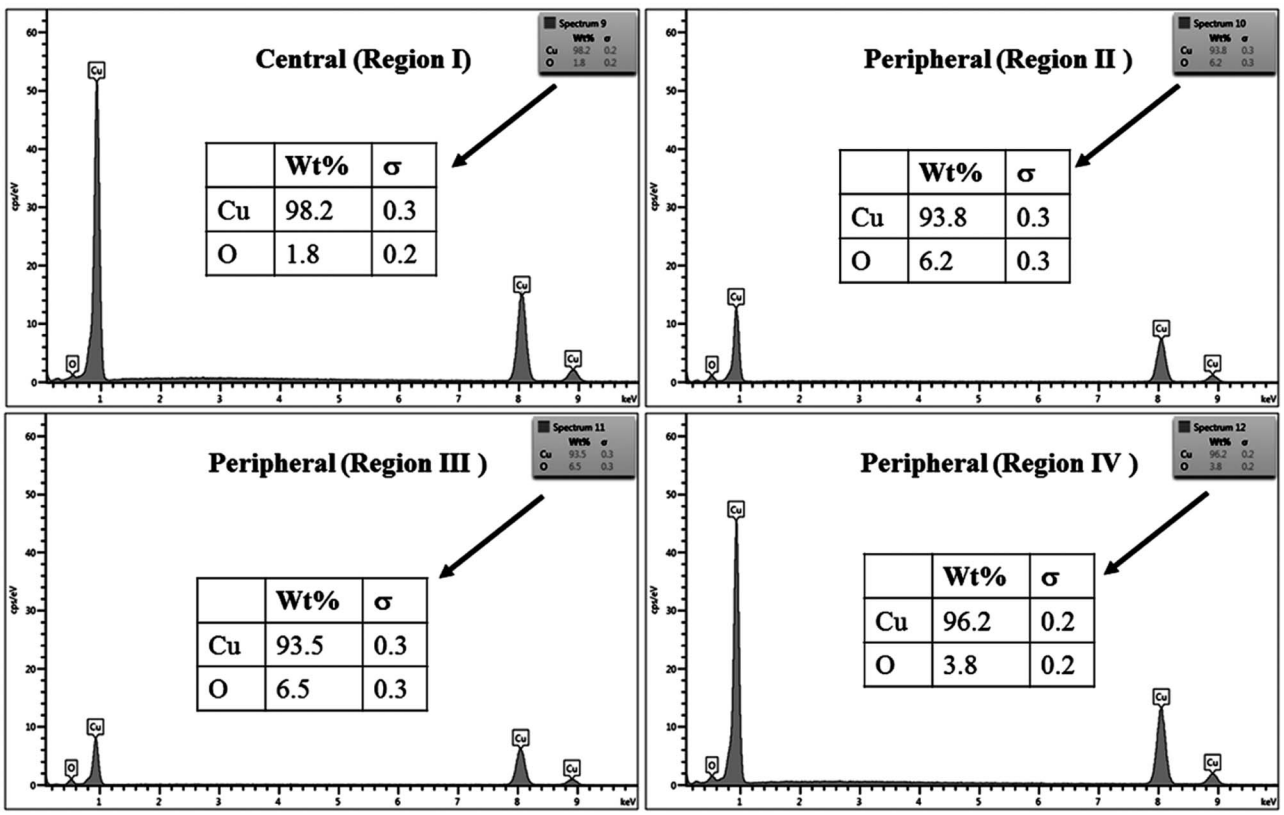

Fig. 9 EDX spectra from different regions of crater produced in air.

XRD and is able to detect the various orientations of oxide phase though it is present in minutest quantity.[28]

Another very important factor responsible in determining the properties of the NPs synthesized *via* PLAL is the dynamics of the cavitation bubbles in liquid.[29] In a recent work by Lam *et al.*, the initial growth and collapse of the cavitation bubbles induced by laser ablation in liquids has been investigated.[30] The behaviour of cavitation bubbles are found to be similar in water, ethanol and isopropanol. Therefore, it can be inferred that in the context of the present work also, the cavitation bubbles affect the properties of the synthesized NPs in a similar manner in all the three liquids.

3.1.2 Surface plasmon resonance of the NPs. The UV-visible absorption spectra of the colloidal solutions of Cu NPs synthesized in methanol and 2-propanol are depicted in Fig. 5(a) and (b), respectively. The SPR peaks of the samples are clearly visible in both the figures.

The SPR peaks vividly reveal a red shift with the increase in irradiation time for the NPs synthesized in both the liquids. For the NPs synthesized in methanol, the SPR peak shifts from ~606 to 621 nm with the increase in ablation duration from 15 to 60 minutes, respectively. This shift is due to the increase in the average size of the NPs from 7 to 19 nm, which was confirmed by the TEM images, Fig. 2. According to Mie theory, there is a peak-shift in an absorption spectrum with the change in the size distribution of the particles.[31] A red shift in the absorption spectrum is generally pertaining to the increase in size of the NPs.[32–34]

In the case of 2-propanol, the SPR peak shifts from ~581 to 601 nm with the increase in ablation duration from 15 to 60 minutes, respectively which is again due to increase in the average size of the NPs from 9 to 17 nm, Fig. 3. The NPs synthesized by pulsed laser ablation in DW as already mentioned, exhibited a blue shift in the SPR peak position with the increase in the laser ablation duration which was confirmed to be due to the reduction in the size of the NPs due to fragmentation for the longer exposure of laser.[26]

As already mentioned, the range of the SPR peak for the NPs synthesized in DW was found to be 626–641 nm[26] whereas that of those synthesized in methanol and 2-propanol are found to be 606–621 nm and 581–601 nm, respectively. From these observations, it is clear that the synthesis of NPs is to a great extent dependent on the surrounding liquid medium. Thus, in order to understand the factors responsible for such observations, there is a need to study the effect of the various ambient on the target surface itself due to laser irradiation. Starting exactly from this, the laser ablated copper target surface in different ambient is analysed and presented in the following section.

3.2 Surface characterization of the laser ablated copper target in different ambient

Once the target is ablated *via* laser, the ablated material condenses in the form of NP leaving behind the cavity or crater on the target in the focal region of the laser beam. The laser produced craters were fabricated using the procedure as

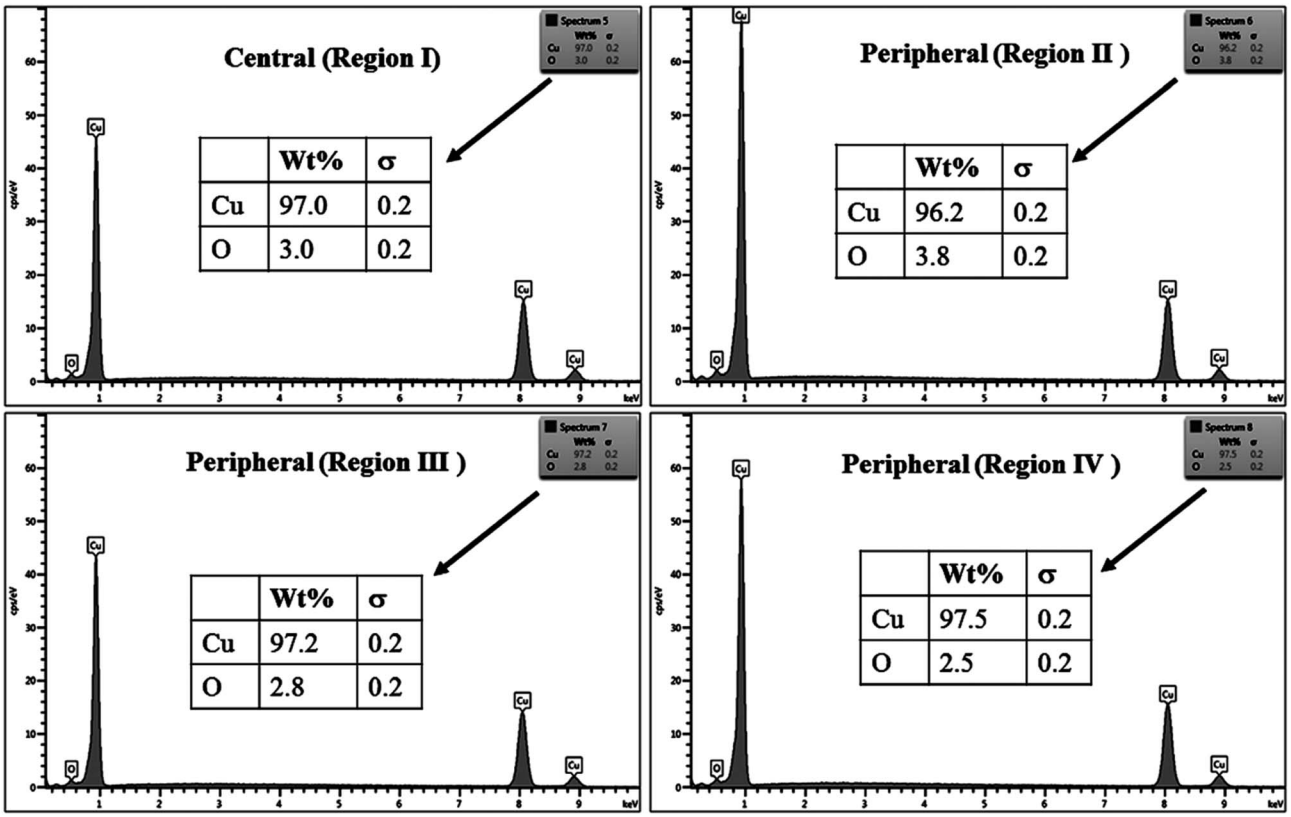

Fig. 10 EDX spectra from different regions of crater produced distilled water.

described in the experimental section in four different ambient, air, DW, methanol and 2-propanol.

3.2.1 Optical microscope images of laser induced crater. The optical micrographs of the laser produced craters in air, DW, methanol and 2-propanol are depicted in Fig. 6(a)–(d), respectively. The crater produced in air is surrounded by a thick blackish envelope. This black envelope is due to the formation of CuO in the sample as a result of excessive aerobic oxidation taking place during ablation in air ambient, Fig. 6(a). The crater produced in DW also shows a darker layer in the peripheral region of the crater but the degree of oxidation is visibly less as compared to that in air, Fig. 6(b).

In the peripheral regions of the craters produced in methanol and 2-propanol, Fig. 6(c) and (d), respectively, there is hardly any blackish layer indicating the absence of CuO phase. However, in both the cases, a blueish envelope along the periphery of the crater is clearly observed which may be due to the formation of oxygen deficient phase of Cu_2O (known to be blue in color). Thus, optical micrographs distinctly indicate the effect of the ambients on the extents of oxidation on the target surface. A better understanding on the formation of Cu_2O and CuO phase could be possible by subjecting the samples to Raman spectroscopic studies as described in the next Subsection, 3.2.2.

3.2.2 Raman analysis of the laser induced crater. In order to verify the observations from the optical micrographs, the ablated surfaces were subjected to Raman spectroscopic measurements. The central region of the crater did not exhibit any Raman peak for any of the surrounding medium. However, the peripheral regions of the craters confirmed the presence of Cu_2O and CuO phases of NPs. For the case of ablation in air, prominent Raman peaks at 292 and 340 cm^{-1} corresponding to A_g and B_g mode, respectively of CuO phase are observed as depicted in Fig. 7(a).[35] The Raman spectrum from the peripheral region of the crater produced in DW, Fig. 7(b), shows peaks at 149, 215 and 293 cm^{-1}.[35] The first two peaks correspond to Cu_2O, while the peak at 293 cm^{-1} corresponds to A_g mode of CuO. The Raman spectra of craters produced in the organic solvents, methanol and 2-propanol shown in Fig. 7(c) and (d), respectively exhibit peaks at 149 and 215 cm^{-1} corresponding to Cu_2O phase. It can be inferred that the periphery of the crater produced in air undergoes maximum oxidation followed by the one produced in DW. Organic solvents being oxygen deficient (also large bond energy of O–H), the peripheral regions of the craters produced in methanol and 2-propanol are least oxidized and exhibited the oxygen deficient phase of Cu oxide. The reproducibility of the observed result is verified by probing different regions of the crater with the micro-Raman laser. Thus, the Raman spectra of the different craters strongly support the predictions based on the optical micrographs of the craters regarding the oxide phase formed.

3.2.3 Energy dispersive X-ray (EDX) of the craters. The optical micrographs of the laser produced craters elucidate the oxide formation around the crater periphery but does not throw any light on the oxide formation in the entire crater region. Also,

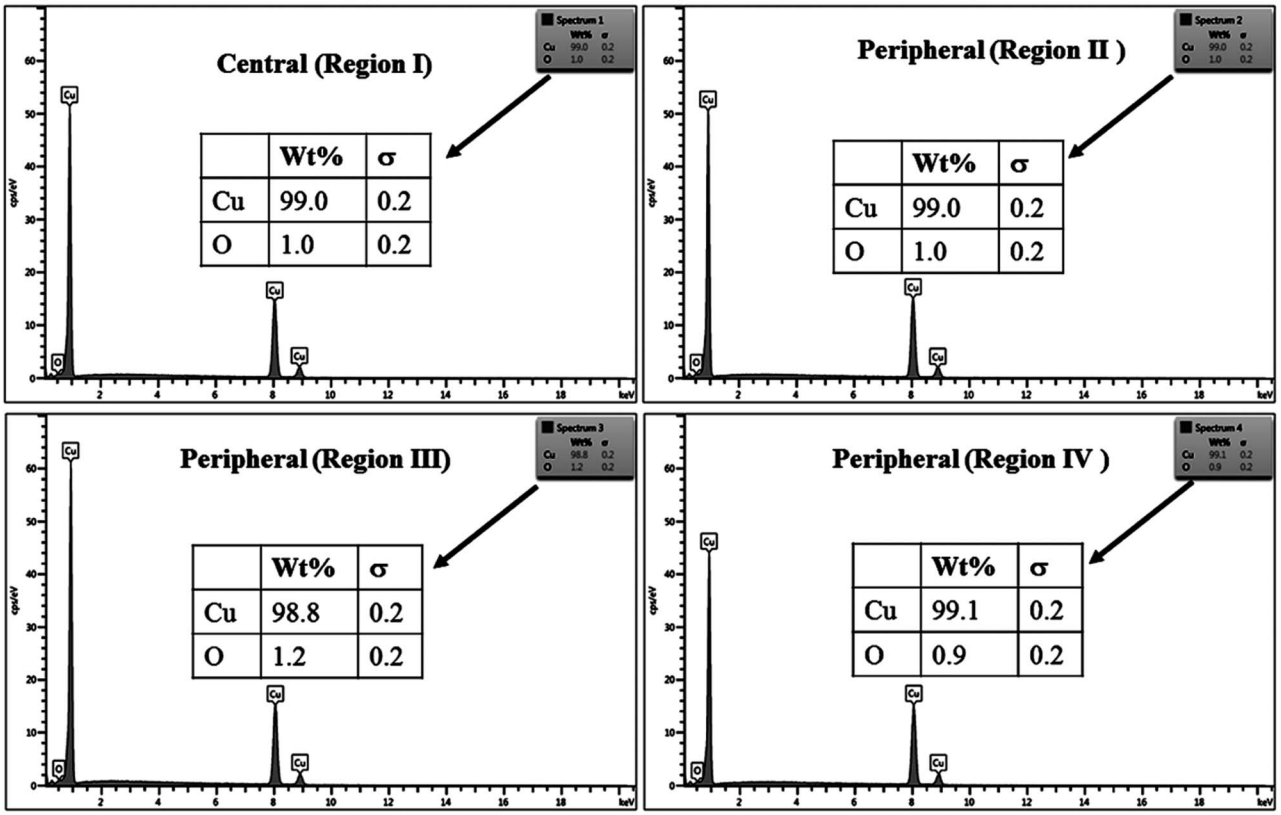

Fig. 11 EDX spectra from different regions of crater produced in air in methanol.

no Raman signal could be detected at the central portion of the craters. Hence, in order to assess the degree of oxidation in the entire crater, all the samples have been subjected to EDX analysis. The percentage of oxygen in different regions of the crater can be a good indication of the oxide formation in the central and peripheral regions of the crater. For this, each and every crater in all the four ambients have been divided into four different regions *viz.*; one central and three peripheral as shown in Fig. 8 (for the crater produced in air, as an example). Similar division of region was also implemented while analysing the craters formed on the Cu target immersed in various liquids.

The % composition of Cu and O along with the EDX spectra of the four regions of the crater in all the samples are shown in Fig. 9–12.

For clarity, the EDX data is also represented graphically in Fig. 13(a)–(d) for the ablation carried out in air, DW, methanol and 2-propanol, respectively. In the central portion of the crater *i.e.* region I, the oxygen content is 1.8, 3.0, 1.0 and 0.6 wt% for air, DW, methanol and 2-propanol, respectively. In the other three regions, the oxygen content is the maximum for ablation in air followed by DW and methanol, and is found to be the least for 2-propanol. The amount of oxygen present in the four representative regions of the craters in the case of ablation in different ambients complements the optical micrographs and Raman spectroscopic analysis.

Except for the central region of the craters, the oxygen content in the peripheral regions decreases in the order: air, DW, methanol, 2-propanol. The % of oxygen for the case of ablation performed in 2-propanol is the least which is due to less oxidation taking place on the target surface. In order to understand this, it is important to investigate the ablation efficiency in each ambient. With this in view, the craters were also subjected to surface profilometer to ascertain the amount of material ablated and hence the ablation rate which is described in the next subsection.

3.2.4 Surface profilometer analysis. In order to assess the mass ablation rate, the volume of the craters has been measured by the surface profilometer. The depth profiles of the craters, shown in Fig. 14(a)–(d), as measured by the surface profilometer, shows that there is change in the depth of the craters produced in different ambients. The depth profiles have been extracted along a line joining two diametrically opposite points on the boundary of the crater. The volumes of the craters produced in air, DW, methanol and 2-propanol are found to be 2.91×10^7, 1.00×10^7, 0.47×10^7, 0.25×10^7 μm^3, respectively. From the volume of the craters, the mass of the material ablated from the target and hence the mass ablation rate (mass ablated per laser shot) was estimated. The mass ablation rate in various ambient is depicted in Fig. 15. The ablation rate is maximum for ablation carried out in air and is minimum for that of in 2-propanol.

There are various factors responsible for the observed reduction in the ablation rate in liquid. With the presence of liquid column above the target, the ablation rate decreases as

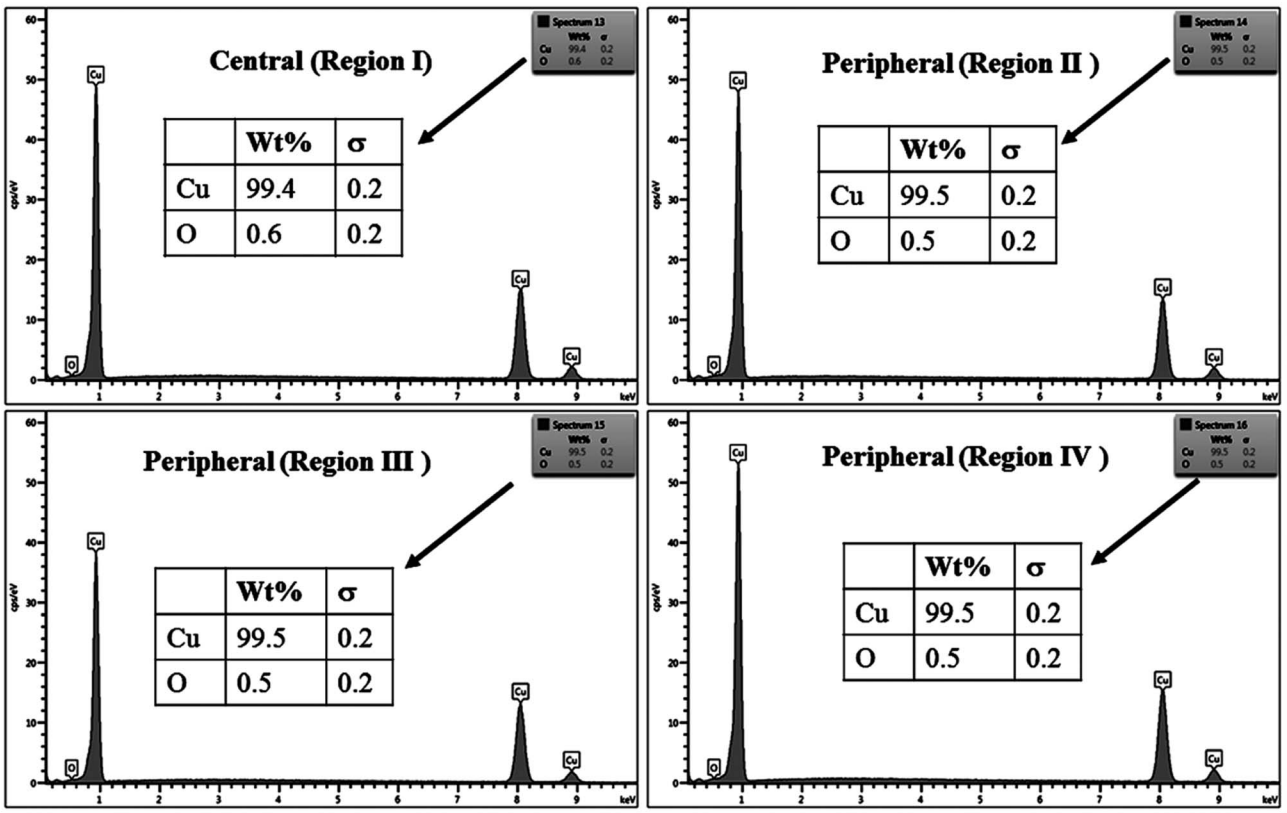

Fig. 12 EDX spectra from different regions of crater produced 2-propanol.

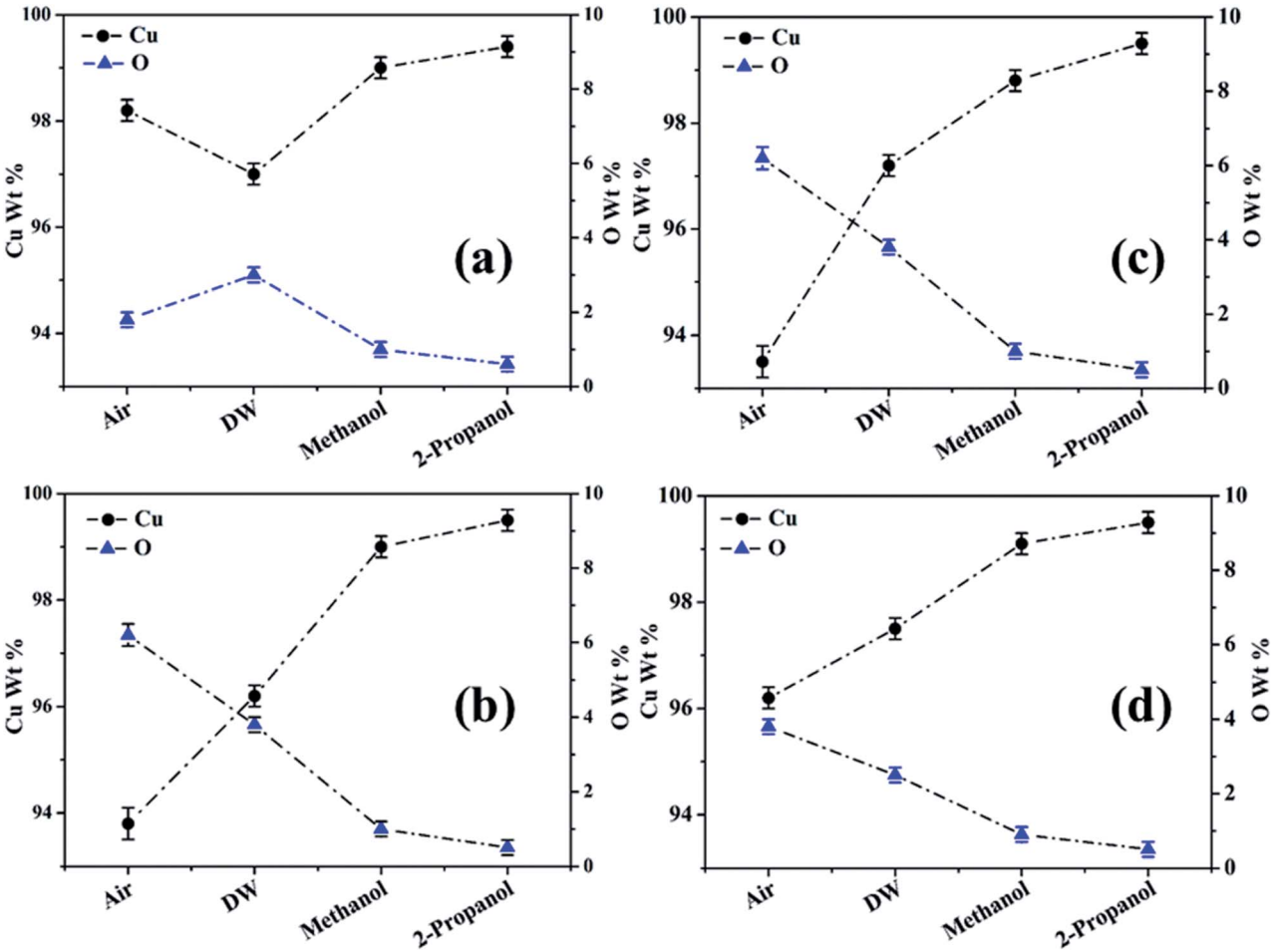

Fig. 13 Graphical representation of the EDX result of craters produced in different ambient for (a) region I, (b) region II, (c) region III and (d) region IV.

there is increased heat loss during as well as after the laser irradiation.[36] This results in a decrease in the temperature and pressure on the target and eventually the process of ablation becomes weaker. In the present case, the height of the liquid column was deliberately kept large as the focussing of the laser beam on the target surface through lower column height of liquid resulted in ignition of methanol and 2-propanol which are flammable liquids. So, the liquid level was maintained at ~4 mm above the target surface for all the three liquids.

The other factors which may equally affect the ablation rate are the various physical properties of the surrounding environment *viz.*, density, thermal conductivity, *etc.* The density of liquids decrease in the order: DW, methanol, 2-propanol. The difference in the density of DW and the two organic solvents is significant while there is only a marginal difference among the densities of the two organic solvents. The maximum density in the case of DW results in strongest liquid-confinement on plasma as compared to that in methanol and 2-propanol.[37] This results in more efficient ablation of the target in DW.

Another reason behind higher ablation rate in DW may be explained by considering the plasma induced recoil pressure. The maximum pressure generated by liquid-confined plasma is given by the following equation:[37,38]

$$P\ (\mathrm{GPa}) = 0.01\sqrt{\frac{\alpha}{\alpha+3}} \times \sqrt{Z\ (\mathrm{g\ cm^{-2}\ s^{-1}})} \times \sqrt{I_0\ (\mathrm{GW\ cm^{-2}})} \quad (1)$$

where α is the fraction of internal energy devoted to thermal energy for ionization (typically $\alpha = 0.1$), I_0 is the incident intensity. The reduced shock impedance, Z between the target and the liquid medium is defined as[37,38]

$$\frac{2}{Z} = \frac{1}{Z_{\mathrm{liquid}}} + \frac{1}{Z_{\mathrm{target}}} \quad (2)$$

where Z_{liquid} and Z_{target} are the acoustic impedances of the surrounding liquid and target, respectively. Thus, the parameter Z takes into consideration the effect of both the surrounding liquid and the target. As α and I_0 are typically same for the ablation carried out in the different liquids, the maximum pressure generated may be considered to be changing with Z as

$$P\ (\mathrm{GPa}) \propto \sqrt{Z} \quad (3)$$

The acoustic impedance of Cu is 4.16×10^6 g cm^{-2} s^{-1} and that of DW, methanol and 2-propanol are listed in Table 1.

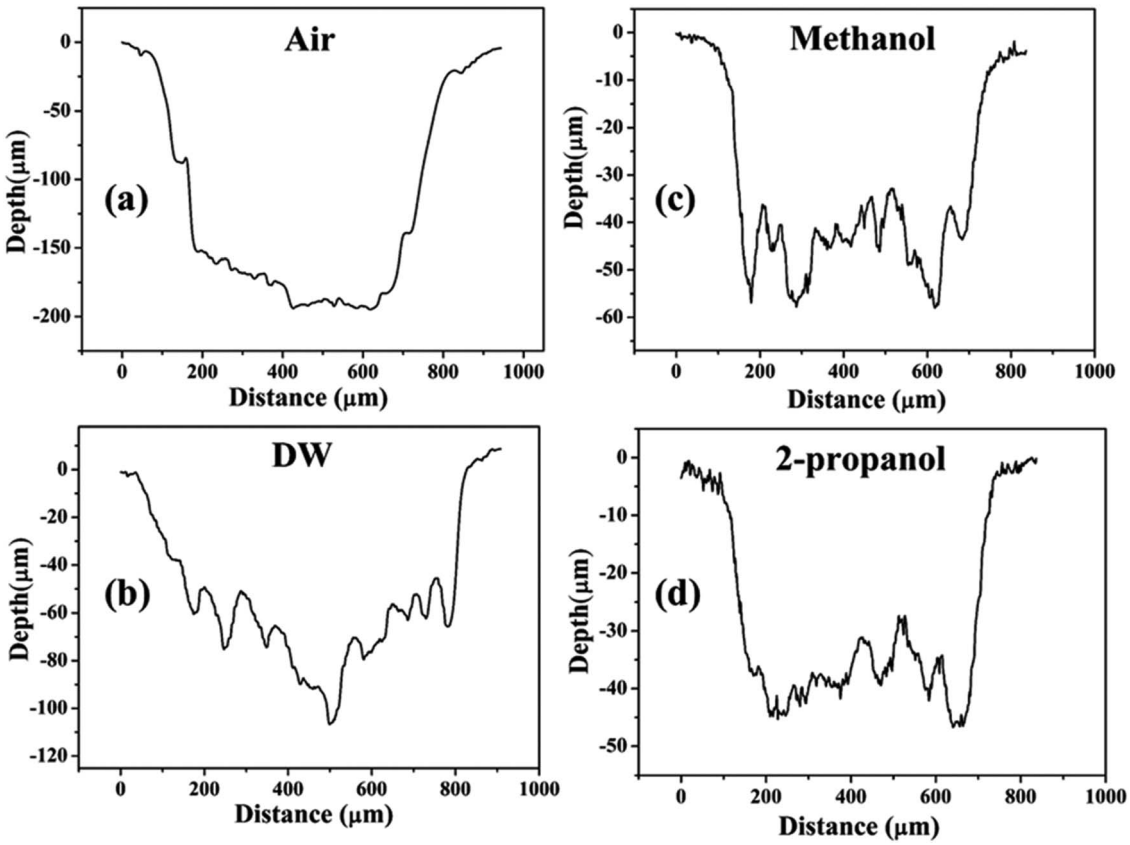

Fig. 14 Depth profiles of the craters produced in (a) air, (b) DW, (c) methanol, and (d) 2-propanol.

Using these values, the value of $\sqrt{Z}$ is evaluated to be ~535, 417 and 424 $g^{1/2}$ cm^{-1} $s^{-1/2}$, respectively. Thus, the maximum pressure generated by DW-confined plasma is very high as compared to those generated by methanol and 2-propanol confined plasmas. Higher plasma induced recoil pressure facilitates more mass removal thereby increasing the ablation rate. Thus, the mass ablation rate is maximum in DW as compared to the two organic liquids and there isn't much difference in the rate of ablation for methanol and 2-propanol.

3.2.5 Surface morphology of the crater using FESEM. The morphology of craters in each case is investigated using the FESEM. Fig. 16(a)–(c) shows the central, the peripheral and magnified image of the peripheral regions, respectively of the crater produced in air, while that of in DW are shown in Fig. 16(d)–(f), respectively.

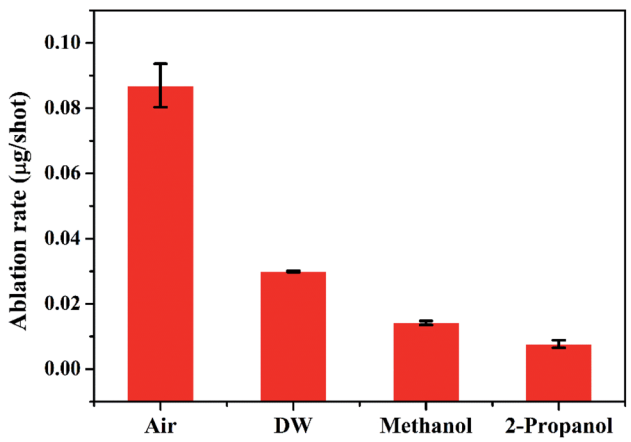

Fig. 15 Variation of mass ablation rate in different ambient.

As the laser beam is focussed onto the target surface, the temperature of the surface increases. Laser ablation in the nanosecond regime is mainly due to photo-thermal process. This may be understood by considering free electrons in the metal target which absorbs the optical energy from the laser radiation and gets excited. The excited electrons impart its excess energy as thermal energy to the lattice *via* non-radiative electron-phonon coupling instantaneously for a nanosecond laser pulse. This results in the energy getting propagated into the solid target and consequently the temperature of the surface increases.[39] Once the ablation threshold of copper is achieved, the material starts getting ablated in the form of hot plasma plume. The laser fluence used in the present case of ablation for Cu in air is ~10 J cm^{-2} which is much above the ablation threshold of 1.6 J cm^{-2} for Cu at laser wavelength of 532 nm. The plasma temperature at this stage is as high as ~9270 and 5798 K in air and water, respectively.[40,41] Due to the achievement of extremely high temperature and pressure regime, evaporation of the target surface takes place leaving behind the molten pool of mass at the centre of the crater. Hence, once the plasma plume is over, for the crater produced in air, the central region consists of mostly melted layers of Cu which solidifies back at

later stage after the termination of the laser pulse. This is evident in the FESEM image (Fig. 16(a)). The fraction of material that ejected out during ablation gets re-deposited onto the target which then re-solidifies and lie along the periphery of the crater in the form of particles as observed in Fig. 16(b) and (c).

The central portion of the crater produced in DW shows similar structure as in air but the melt-like structure is less prominent (Fig. 16(d)). This is because the surrounding DW cools down the target surface much faster by absorbing most of the heat from the target surface.[42] The origin of this rapid decrease of temperature lies in the high thermal conductivity of water compared to that of air which results in more heat

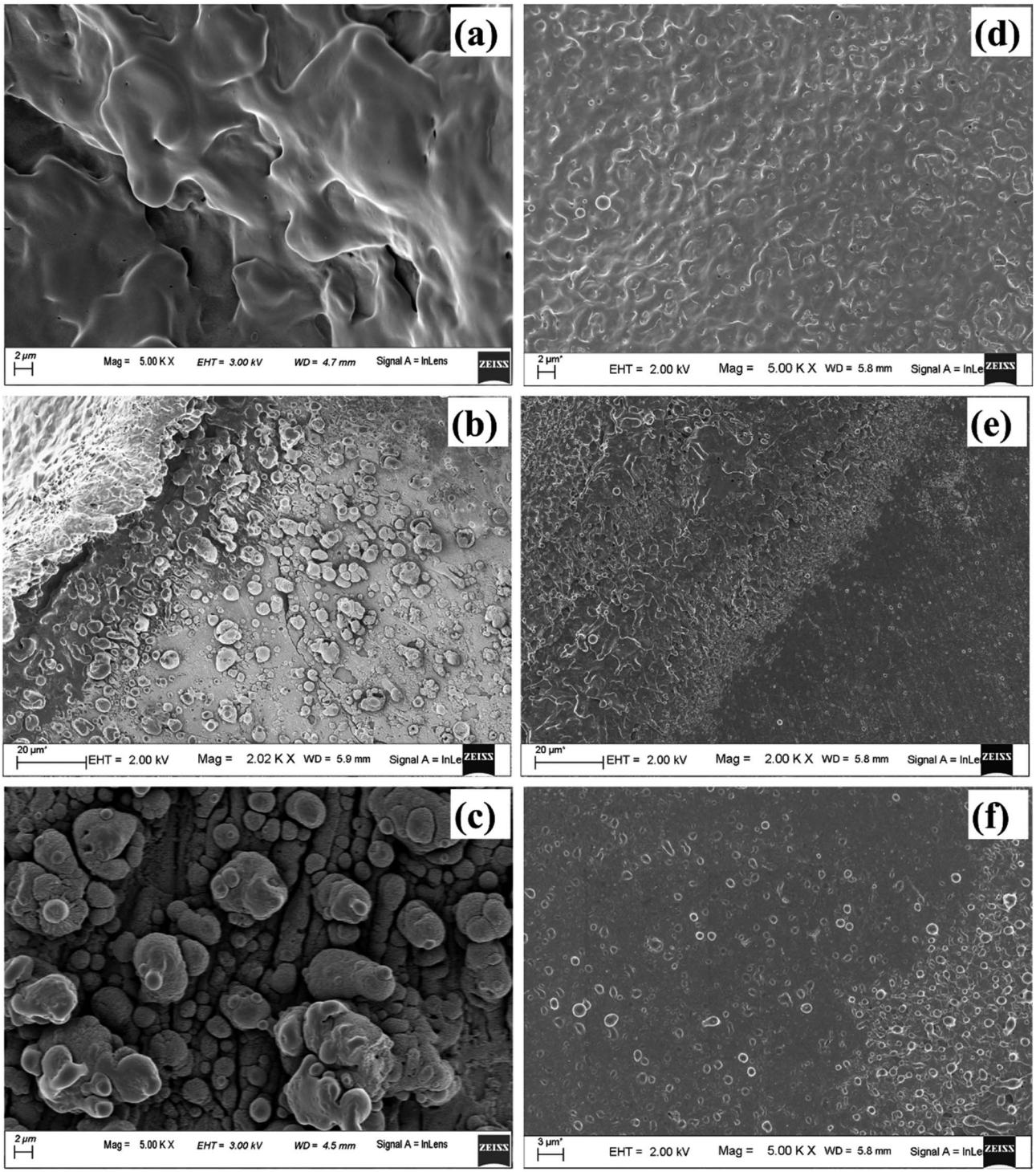

Fig. 16 FESEM image of (a)–(c) central, peripheral and the magnified image of the peripheral region, respectively of laser produced crater in air, (d)–(f) respective images of the crater produced in DW.

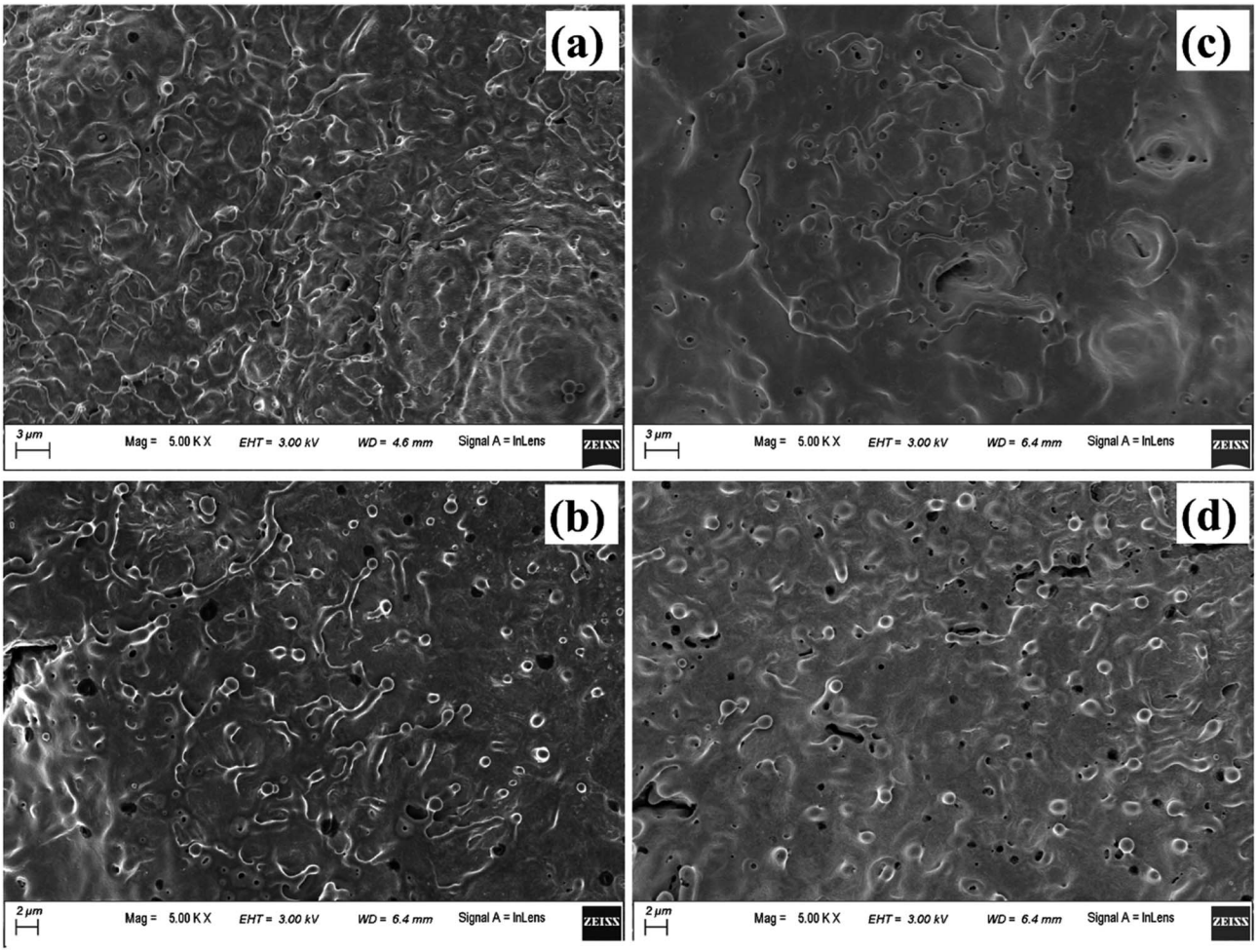

Fig. 17 FESEM image of (a) and (b) central and peripheral region, respectively of laser produced crater in methanol, (c) and (d) respective images of the crater produced in 2-propanol.

transfer in DW and hence a decrease in the plasma temperature. During ablation in DW, dissociation of the water molecules produces hydrogen and oxygen gas. As the thermal conductivity of hydrogen gas (0.187 W mK^{-1}) is much larger than that of air (0.026 W mK^{-1}) so the release of hydrogen gas facilitates faster cooling in DW.[40] So, the heat affected zone formed in the case of ablation in DW is less, thereby making the molten structures, formed in the central part of the crater, less prominent. The molten material at the centre of the crater splashes out due to the high pressure and is redeposited in the radially outward direction which is visible in the peripheral region of the crater shown in Fig. 16(e) and (f). Also, unlike in air, there are only a few particles present along the periphery of the crater in DW as most of the molten material is washed away and remain suspended in the DW in the form of NPs.

Fig. 17(a), (b) and (c), (d) depict the central and peripheral regions, of the crater produced in methanol and 2-propanol, respectively. For the craters produced in both these organic solvents, the central region is dominated by thin layers of solidified melt similar to that observed in DW. However, there is appearance of small micro pores as observed in Fig. 17(a) and (c). There are reports of formation of micro pores due to etching action of organic solvents on the target surface during laser ablation.[42] This strong etching property of methanol and 2-propanol may result in the formation of micro-pores on the surface of the target. Again, it is observed that the number of such micro pores are slightly more in the case of 2-propanol than in methanol. During plasma formation, the pressure created in the focal volume of the laser beam is enormously high and at higher pressure, 2-propanol is known to have higher etch rate than methanol.[43] This must be the possible reason for observing more number of micro-pores for the ablation carried in 2-propanol. The periphery of the craters in methanol and 2-propanol are found to exhibit similar structure to that of the crater produced in DW. Moreover, the micro-pores which were observed in the central part are also found in the peripheral regions.

Another possible reason for the formation of the micro-pores could be the volatile nature of the organic solvents. Due to this, during laser ablation, as the laser beam passes through the organic liquids, it is observed that the target plasma sometimes induces excess breakdown of the liquid and there is a cracking sound. This is due to a phase explosion taking place and as a result there is violent disturbance in the ejected material which is in the molten state. The molten mass cools and re-

solidifies immediately but the imprint of the violent disturbance in the form of micro-pores remains embedded on it.

4. Conclusion

Insufficiently oxidized Cu NPs have been synthesized by pulsed laser ablation of Cu target immersed in methanol and 2-propanol. The size of the NPs increases with the increase in the laser irradiation time and there is corresponding redshift in the plasmonic peak in both the solvents. This behaviour is in sharp contrast to the NPs synthesized in DW. Oxidation of the NPs is found to be minimal for the synthesis of NPs in the organic solvents than that in DW. Carbon encapsulation of the NPs resulting in core–shell NPs is a reason behind the decrease in the oxidation occurring in the organic solvents. The ablation study of the laser produced crater in different ambient reveals that the process of laser ablation is dependent on the properties of the surrounding medium to a great extent. There are remarkable changes in the structural and morphological features of the target surface when the ablation is carried out in different ambient. The ablation in air resulted in the formation of big sized NPs deposited on the target surface. In liquid ambient, the synthesized NPs remain suspended in the surrounding liquid. It is also observed that cleaner surface with minimum amount of micro or nanoparticles are obtained for the laser ablated surface in liquids as compared to that of air. This may help in the fabrication of clean channels in laser induced micromachining. From the viewpoint of NP synthesis, the variation in the degree of oxidation of the NPs may be related to the less oxidation of the target surface in organic solvents as compared to DW and air, in addition to its encapsulation by carbon.

Conflicts of interest

There are no conflicts to declare.

Acknowledgements

The authors acknowledge the Central Instruments Facility (CIF), IIT Guwahati for the FESEM, EDX, TEM and micro-Raman facility. The authors also acknowledge the Advanced Manufacturing Laboratory, Mechanical Engineering department, IIT Guwahati for the surface profilometer facility. Department of Science and Technology (India), Project No. SR/S2/HEP-18/2009 is also acknowledged.

References

1 A. Zaleska-Medynska, M. Marchelek, M. Diak and E. Grabowska, *Adv. Colloid Interface Sci.*, 2016, **229**, 80–107.
2 C. Clavero, *Nat. Photonics*, 2014, **8**, 95.
3 X. Huang, H. Yu, H. Tan, J. Zhu, W. Zhang, C. Wang, J. Zhang, Y. Wang, Y. Lv and Z. Zeng, *Adv. Funct. Mater.*, 2014, **24**, 6516–6523.
4 J. Liu, W. Wang, T. Shen, Z. Zhao, H. Feng and F. Cui, *RSC Adv.*, 2014, **4**, 30624–30629.
5 M. Li, S. K. Cushing and N. Wu, *Analyst*, 2015, **140**, 386–406.
6 P. Gao and D. Liu, *Sens. Actuators, B*, 2015, **208**, 346–354.
7 M. Karami, M. Akhavan-Behabadi, M. R. Dehkordi and S. Delfani, *Sol. Energy Mater. Sol. Cells*, 2016, **144**, 136–142.
8 G. Li, M. Jing, Z. Chen, B. He, M. Zhou and Z. Hou, *RSC Adv.*, 2017, **7**, 10376–10384.
9 X. Liu, J. Chen, P. Liu, H. Zhang, G. Li, T. An and H. Zhao, *Appl. Catal., A*, 2016, **521**, 34–41.
10 S. Chatterjee and A. J. Pal, *J. Phys. Chem. C*, 2016, **120**, 1428–1437.
11 S. Shinde, H. Dhaygude, D.-Y. Kim, G. Ghodake, P. Bhagwat, P. Dandge and V. Fulari, *J. Ind. Eng. Chem.*, 2016, **36**, 116–120.
12 J. Zhang, J. Liu, Q. Peng, X. Wang and Y. Li, *Chem. Mater.*, 2006, **18**, 867–871.
13 J. Choi, H. Oh, S.-W. Han, S. Ahn, J. Noh and J. B. Park, *Curr. Appl. Phys.*, 2017, **17**, 137–145.
14 J. Ruusunen, M. Ihalainen, T. Koponen, T. Torvela, M. Tenho, J. Salonen, O. Sippula, J. Joutsensaari, J. Jokiniemi and A. Lähde, *J. Nanopart. Res.*, 2014, **16**, 2270.
15 S. Jeong, K. Woo, D. Kim, S. Lim, J. S. Kim, H. Shin, Y. Xia and J. Moon, *Adv. Funct. Mater.*, 2008, **18**, 679–686.
16 H. Zeng, X. W. Du, S. C. Singh, S. A. Kulinich, S. Yang, J. He and W. Cai, *Adv. Funct. Mater.*, 2012, **22**, 1333–1353.
17 D. Zhang, B. Gökce and S. Barcikowski, *Chem. Rev.*, 2017, **117**, 3990–4103.
18 P. Liu, H. Wang, X. Li, M. Rui and H. Zeng, *RSC Adv.*, 2015, **5**, 79738–79745.
19 M. Muniz-Miranda, C. Gellini, A. Simonelli, M. Tiberi, F. Giammanco and E. Giorgetti, *Appl. Phys. A: Mater. Sci. Process.*, 2012, **110**, 829–833.
20 A. Baladi and R. Sarraf Mamoory, *Appl. Surf. Sci.*, 2010, **256**, 7559–7564.
21 A. Kanitz, J. S. Hoppius, M. del Mar Sanz, M. Maicas, A. Ostendorf and E. L. Gurevich, *ChemPhysChem*, 2017, **18**, 1155–1164.
22 R. M. Tilaki, A. Iraji zad and S. M. Mahdavi, *Appl. Phys. A: Mater. Sci. Process.*, 2007, **88**, 415–419.
23 Y. Han, R. Lupitskyy, T.-M. Chou, C. M. Stafford, H. Du and S. Sukhishvili, *Anal. Chem.*, 2011, **83**, 5873–5880.
24 B. Kumar, D. Yadav and R. K. Thareja, *J. Appl. Phys.*, 2011, **110**, 074903.
25 J. Lam, D. Amans, F. Chaput, M. Diouf, G. Ledoux, N. Mary, K. Masenelli-Varlot, V. Motto-Ros and C. Dujardin, *Phys. Chem. Chem. Phys.*, 2014, **16**, 963–973.
26 P. K. Baruah, A. K. Sharma and A. Khare, *Opt. Laser Technol.*, 2018, **108**, 574–582.
27 H. Zeng, S. Yang and W. Cai, *J. Phys. Chem. C*, 2011, **115**, 5038–5043.
28 D. B. Williams and C. B. Carter, in *Transmission Electron Microscopy: A Textbook for Materials Science*, Springer US, Boston, MA, 2009, pp. 197–209, DOI: 10.1007/978-0-387-76501-3_11.
29 M. Dell'Aglio, R. Gaudiuso, O. De Pascale and A. De Giacomo, *Appl. Surf. Sci.*, 2015, **348**, 4–9.
30 J. Lam, J. Lombard, C. Dujardin, G. Ledoux, S. Merabia and D. Amans, *Appl. Phys. Lett.*, 2016, **108**, 074104.

31 G. Mie, *Ann. Phys.*, 1908, **25**, 377–445.
32 A. Takami, H. Kurita and S. Koda, *J. Phys. Chem. B*, 1999, **103**, 1226–1232.
33 S. Link and M. A. El-Sayed, *J. Phys. Chem. B*, 1999, **103**, 8410–8426.
34 U. Kreibig and M. Vollmer, *Optical properties of metal clusters*, Springer Science & Business Media, 2013.
35 A. S. Zoolfakar, R. A. Rani, A. J. Morfa, A. P. O'Mullane and K. Kalantar-zadeh, *J. Mater. Chem. C*, 2014, **2**, 5247–5270.
36 H. W. Kang and A. J. Welch, *J. Appl. Phys.*, 2007, **101**, 083101.
37 P. Ouyang, P. Li, E. Leksina, S. Michurin and L. He, *Appl. Surf. Sci.*, 2016, **360**, 880–888.
38 S. Zhu, Y. Lu, M. Hong and X. Chen, *J. Appl. Phys.*, 2001, **89**, 2400–2403.
39 J. Yu, Q. Ma, V. Motto-Ros, W. Lei, X. Wang and X. Bai, *Front. Phys.*, 2012, **7**, 649–669.
40 B. Kumar and R. K. Thareja, *Phys. Plasmas*, 2013, **20**, 053503.
41 M. Sabsabi and P. Cielo, *J. Anal. At. Spectrom.*, 1995, **10**, 643–647.
42 V. Tangwarodomnukun and H.-Y. Chen, *Mater. Manuf. Processes*, 2015, **30**, 685–691.
43 K. Torek, J. Ruzyllo, R. Grant and R. Novak, *J. Electrochem. Soc.*, 1995, **142**, 1322–1326.